JPE 15-3-22

http://dx.doi.org/10.6113/JPE.2015.15.3.796
ISSN(Print): 1598-2092 / ISSN(Online): 2093-4718

Control Method for Fault-Tolerant Active Power Filters

Chenyu Zhang*, Jianyong Zheng†, Jun Mei*, Kai Deng*, and Fuju Zhou*

*†School of Electrical Engineering, Southeast University, Nanjing, China

Abstract

New direct and indirect current control methods for a fault-tolerant active power filter topology are presented in this paper. Since a three-phase four-switch topology has a phase bridge current which cannot be directly controlled, a hysteresis control method in the α-β plane which controls the three-phase current in the two-phase stationary coordinate system is proposed. The improved SVPWM algorithm is able to eliminate the operation of the trigonometric functions in the traditional algorithm by rotating the α-β coordinates and alternating the sequence of the output vectors, which in turn simplifies the algorithm and reduces the switching frequency. The selection of the DC-side reference voltage and DC-side capacitor equalization strategy are also discussed. Simulation and experiments demonstrate that the proposed control method is correct and feasible.

Key words: Active Power Filter (APF), DC-side voltage, Fault tolerant, Hysteresis control, Space vector modulation

I. INTRODUCTION

As a result of the intensive growth of the power quality problems in power systems, the active power filter (APF) has been widely studied and applied as a dynamic shunt compensation device due to its real time harmonic and reactive power compensation [1]-[4]. However, since an APF usually operates in harsh industrial environments with high temperatures in which the power switching device IGBT runs at a high frequency, reliable operation of the power switching device is required to guarantee the stability of the APF [5]. Once the IGBT breaks down due to overvoltage or overcurrent, the general approach is to remove the APF from the grid and wait for repair. With the appearance of the three-phase four-switch APF (TFSSAPF), an APF can continue to operate effectively and reliably by changing its topology when a single-phase power device is dysfunctional. This gives the APF a certain amount of self-healing capability, extends the APF work period and buys more time for fault handling.

The conventional three-phase six-switch APF has been studied a lot since the 1980s [6]-[9], and its control algorithms have been completely developed. Therefore, it does not need to be repeated in this paper. However, the three-phase four-switch APF control strategy within a fault-tolerant topology has not been thoroughly studied. Since the shunt grid voltage source inverter (VSI) control methods are mainly divided into direct current control and indirect current control, new direct and indirect control schemes for the TFSSAPF topology are proposed in this paper.

For the direct control method, a hysteresis current control in the α-β coordinate system for the TFSSAPF is proposed. Since the TFSSAPF has a direct connection between the phase bridge and the midpoint of the DC side, the phase current is no longer independently controlled. In the proposed method, two hysteresis comparators separately control the two-phase stationary coordinates on the α-β axes. Then the overall control of the abc three-phase current is achieved.

For the indirect control method, some studies [10]-[14] analyze the three-phase four-switch inverter fault-tolerant control strategy. The study in [15] introduces this kind of control strategy to the control of an APF and the study in [16] discusses the operation of a TFSSAPF when the three-phase grid voltage is unbalanced and the grid is under a short-time fault. However, in these papers the sector of the vector is classified by the phase angle of the reference vector, which requires a massive trigonometric function calculation. In order to avoid the use of a look-up table by the digital processor to obtain the trigonometric calculation results and to get the sector number through the positive and negative values of the line

Manuscript received Apr. 28, 2014; accepted Jan. 24, 2015
Recommended for publication by Associate Editor Kyo-Beum Lee.
†Corresponding Author: zhengjy_seu@163.com
Tel: +86-15205159699, Southeast University
*School of Electrical Engineering, Southeast University, China

voltage in the same way as the three-phase six-switch APF, the study in [17] greatly reduces the complexity of the algorithm by means of vector rotation. Based on that, the study in [18] proposes a five-segment-type SVPWM modulation algorithm. Based on former studies, an improved SVPWM modulation algorithm for the TFSSAPF is proposed in this paper. First, the α-β coordinates are rotated 120° clockwise to obtain the g-h coordinates to coincide the basic vectors with the new axes. In this way, the sector of the reference vector can be directly determined through the basic operations of the line voltage, which saves a lot of trigonometric calculations in the traditional α-β coordinate system. Then the five-segment-type SVPWM modulation algorithm described in [18] is further improved so that only one phase switching state changes within each sector to simplify the algorithm and to reduce the switching frequency.

In addition, for the DC-side capacitor voltage control, this paper discusses the selection of the initial value of the DC-side voltage for the TFSSAPF and the solution of the capacitors voltage equalization. Finally, simulations and experiments which verify both the correctness and feasibility of this algorithm are presented.

This paper is organized as follows. Fault tolerance mechanisms for APFs are reviewed in Section II. A current control scheme for the TFSSAPF is presented in Section III. A DC voltage control scheme is illustrated in Section IV. Simulation and experimental results are given in Section V.

II. Fault Tolerance Mechanisms

Since they are operated in special industrial field environments, IGBT are vulnerable devices in extreme working conditions in which the fault detection and tolerance mechanism of the APF is an essential element. A three-phase four-switch APF tolerant topology circuit is introduced in this paper. It is a fault-tolerant solution when one phase power device of the APF opens circuit under normal operating conditions (when IGBT short circuits due to the breakdown of each series of fast fuse switches immediately disconnect the phase, so that in this article it will be considered as a phase IGBT short circuit breaker) is given. Fig. 1(a) shows the APF tolerant topology, where KM_1, KM_3, and KM_5 are open contactors; KM_2, KM_4, and KM_6 are close contactors; and $S_1 \sim S_6$ are six-leg three-phase power switches. When S_5 or S_6 fails in phase c, the c-phase bridge connects to the middle of the DC-side capacitors so that the APF topology is changed from Fig. 1(b) to Fig. 1(c).

In Fig. 1, the TFSSAPF reduces one phase bridge arm which in turn decreases the number of switching states from six to four. This inevitably leads to a lower modulation accuracy, but also reduces the cost of the power switches and drivers. As a fault-tolerant solution, it extends the lifetime of the APF which gives it research and application potential.

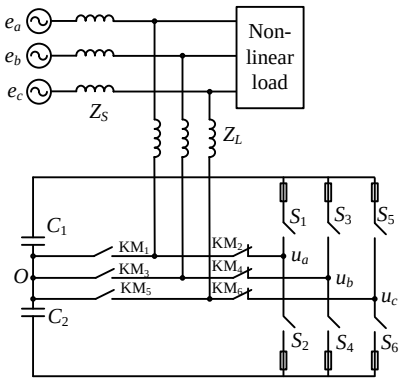

(a) Topology of fault-tolerant APF.

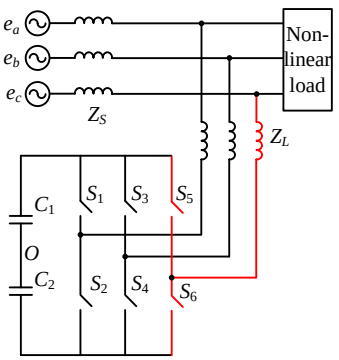

(b)Normal topology of APF.

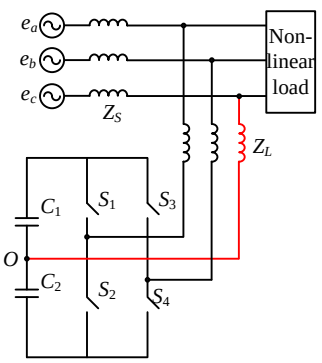

(c) Topology of TFSSAPF.

Fig. 1. Fault-tolerant topology of APF.

III. Current Control Schemes

When an APF encounters a single phase open circuit fault, it automatically cuts the damaged phase current through a self-fault diagnosis in which the topology switches to a three-phase four-switching state. Due to this change, the current control scheme is no longer the same as the traditional three-phase six-switch topology.

A. Hysteresis Control

When a c-phase circuit experiences an open-circuit fault, the topology circuit is switched to the three-phase four-switching state. When the DC-side capacitor voltage control is at the steady state and the capacitor voltage is

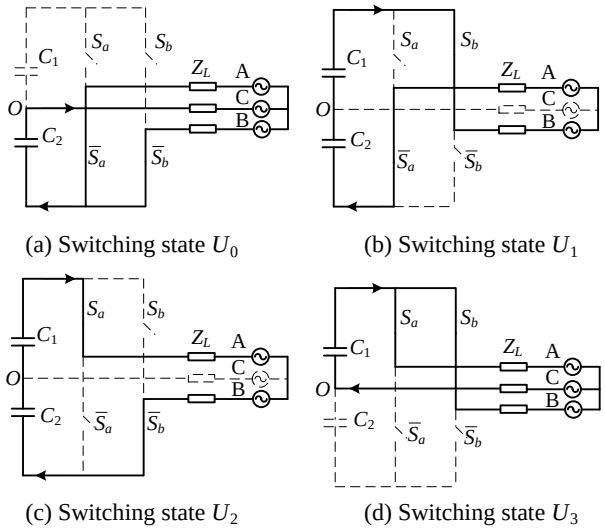

(a) Switching state U_0 (b) Switching state U_1

(c) Switching state U_2 (d) Switching state U_3

Fig. 2. Switching status of TFSSAPF.

equalized such that $u_{c1}=u_{c2}=u_{dc}/2$, only the output line voltages u_{ao} and u_{bo} can be directly controlled since the c-phase bridge is connected to the middle of the DC-side capacitors. Each of the switching state diagrams is shown in Fig. 2(a)-(d).

When the switch of S_a and S_b is open, it is equal to 1 and vice versa. Then, the switching states of the TFSSAPF can be described as:

$$\begin{bmatrix} u_{ao} \\ u_{bo} \end{bmatrix} = \frac{u_{dc}}{2}\begin{bmatrix} 2S_a - 1 \\ 2S_b - 1 \end{bmatrix} \tag{1}$$

The stationary three-phase coordinates can be transformed to α-β coordinate as:

$$U = u_\alpha + \mathrm{j}u_\beta = \sqrt{\frac{2}{3}}(u_a + u_b e^{\mathrm{j}\frac{2}{3}\pi} + u_c e^{\mathrm{j}\frac{2}{3}\pi}) \tag{2}$$

Equation (2) can be written in a matrix as:

$$\begin{bmatrix} u_\alpha \\ u_\beta \end{bmatrix} = C_{abc-\alpha\beta}\begin{bmatrix} u_{ao} \\ u_{bo} \\ u_{co} \end{bmatrix} \tag{3}$$

Where:

$$C_{abc-\alpha\beta} = \sqrt{\frac{2}{3}}\begin{bmatrix} 1 & -1/2 & -1/2 \\ 0 & \sqrt{3}/2 & -\sqrt{3}/2 \end{bmatrix} \tag{4}$$

Since output voltage u_{oc} is always 0, combining equation (1) with equation (3) yields:

$$\begin{bmatrix} u_\alpha \\ u_\beta \end{bmatrix} = \frac{u_{dc}}{\sqrt{6}}\begin{bmatrix} 1 & -1/2 \\ 0 & \sqrt{3}/2 \end{bmatrix}\begin{bmatrix} 2S_a - 1 \\ 2S_b - 1 \end{bmatrix} \tag{5}$$

Equation (5) gives the relationship between the switching signals and voltage space vectors in the α-β coordinate system as shown in Table I.

The new APF topology cannot control the c-phase output current independently. Therefore, three independent

TABLE I

RELATIONSHIP BETWEEN SWITCHING SIGNALS AND VOLTAGE SPACE VECTORS IN α-β COORDINATE

U_k	S_a	S_b	U_{ao}	U_{bo}	U_α	U_β
U_0	0	0	$-U_{dc}/2$	$-U_{dc}/2$	$-U_{dc}/2\sqrt{6}$	$-U_{dc}/2\sqrt{2}$
U_1	0	1	$-U_{dc}/2$	$U_{dc}/2$	$-3U_{dc}/2\sqrt{6}$	$U_{dc}/2\sqrt{2}$
U_2	1	0	$U_{dc}/2$	$-U_{dc}/2$	$3U_{dc}/2\sqrt{6}$	$-U_{dc}/2\sqrt{2}$
U_3	1	1	$U_{dc}/2$	$U_{dc}/2$	$U_{dc}/2\sqrt{6}$	$U_{dc}/2\sqrt{2}$

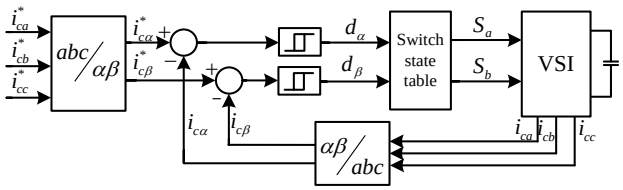

Fig. 3. Diagram of hysteresis control in α-β coordinate.

TABLE II

SWITCHING STATE TABLE

d_α	d_β	U_k	S_a	S_b
-1	-1	U_0	0	0
-1	+1	U_1	0	1
+1	-1	U_2	1	0
+1	+1	U_3	1	1

hysteresis comparator cannot be used to control the three-phase current. A hysteresis current control method in α-β coordinate system for the TFSSAPF is proposed in this paper, where the hysteresis controls the α-β axis in the two-phase stationary coordinate system in order to achieve complete control of the abc three-phase current. A diagram of the hysteresis control in α-β coordinate system is shown in Fig. 3.

Table I and Fig. 3 are combined and the α-axis is taken as an example. When the actual output current is greater (less) than the reference value, d_α = -1 (1), the output of the α-axis need a negative (positive) voltage to reduce (increase) the actual output current. This is similar to the β-axis control principle. Therefore, the hysteresis output state d_α, d_β in the α-β coordinate system determines the switching state U_k which is shown in Table II.

Hysteresis control in the α-β coordinate system for the TFSSAPF effectively solves the problem of a phase current connection with a midpoint of the output capacitor that cannot be directly controlled. The control method has excellent dynamic response. However, the compensation precision and switching frequency are affected by the width of the hysteresis ring.

B. SVPWM Control

According to Table I, the TFSSAPF basic output voltage space vector in the α-β coordinate system is not on the basic axes. This leads to the need for a α-β component projection of the reference voltage vector to the direction of the basic space

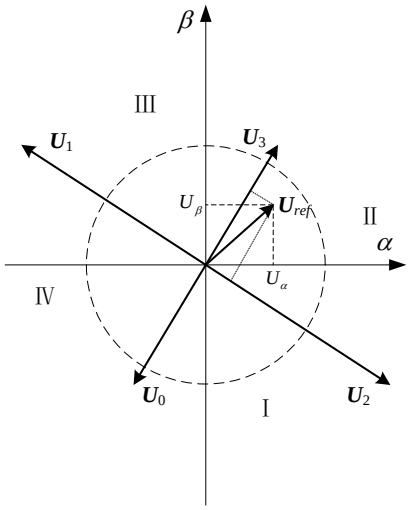

(a) α-β coordinate.

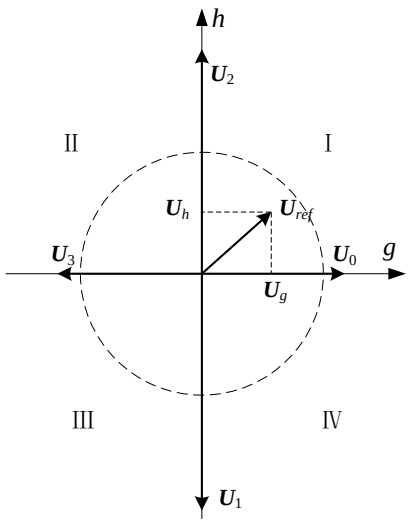

(b) *g-h* coordinate.

Fig. 4. Distribution diagram of the basic voltage space vectors.

vector. This process requires a lot of phase transformation and trigonometric function operations. In order to simplify the SVPWM control method, the α-β coordinates are rotated 120° clockwise to obtain the *g-h* coordinates so that the basic vector U_0 coincides with the positive g-axis, while the reference voltage vector is projected to the *g-h* coordinates for operation, which is shown in Fig. 4.

According to Fig. 4(b), the three phase stationary coordinate is projected to *g-h* coordinate system so that:

$$U = u_g + \mathrm{j}u_h = \sqrt{\frac{2}{3}}(u_a e^{\mathrm{j}\frac{2}{3}\pi} + u_b e^{\mathrm{j}\frac{4}{3}\pi} + u_c) \quad (6)$$

Equation (6) can be written in matrix form as:

$$\begin{bmatrix} u_g \\ u_h \end{bmatrix} = C_{abc-gh} \begin{bmatrix} u_{ao} \\ u_{bo} \\ u_{co} \end{bmatrix} \quad (7)$$

TABLE III
RELATIONSHIP BETWEEN SWITCHING SIGNALS AND VOLTAGE SPACE VECTORS IN *g-h* COORDINATE

U_k	S_a	S_b	U_{ao}	U_{bo}	U_g	U_h
U_0	0	0	$-U_{dc}/2$	$-U_{dc}/2$	$U_{dc}/\sqrt{6}$	0
U_1	0	1	$-U_{dc}/2$	$U_{dc}/2$	0	$-U_{dc}/\sqrt{2}$
U_2	1	0	$U_{dc}/2$	$-U_{dc}/2$	0	$U_{dc}/\sqrt{2}$
U_3	1	1	$U_{dc}/2$	$U_{dc}/2$	$-U_{dc}/\sqrt{6}$	0

Where:

$$C_{abc-gh} = \sqrt{\frac{2}{3}} \begin{bmatrix} -1/2 & -1/2 & 1 \\ \sqrt{3}/2 & -\sqrt{3}/2 & 0 \end{bmatrix} \quad (8)$$

In addition, it is assumed that c-phase current is under a fault and that u_{co} is always 0. Combining equation (1) with (7) yields:

$$\begin{bmatrix} u_g \\ u_h \end{bmatrix} = \frac{u_{dc}}{\sqrt{6}} \begin{bmatrix} -1/2 & -1/2 \\ \sqrt{3}/2 & -\sqrt{3}/2 \end{bmatrix} \begin{bmatrix} 2S_a - 1 \\ 2S_b - 1 \end{bmatrix} \quad (9)$$

Equation (9) gives the relationship between the switching signals and the voltage space vectors in *g-h* coordinate system as Table III.

In the α-β coordinate system, the angle of the reference vector should be calculated first to determine the sector. However, in the *g-h* coordinate system the sector can be directly obtained by looking at the signs of u_g and u_h as shown in Fig. 4(b). This improvement greatly reduces the amount of arithmetic operations.

Due to the absence of a zero sequence current component in the three-phase three-wire system and the three-phase asymmetry, the output voltage can be decomposed into positive sequence component and negative sequence component, as shown in Fig. 5. When the TFSSAPF equivalent output requires the three-phase positive sequence components, the vector diagram is shown in Fig. 5(c).

According to Fig. 5(c), the following is obtained:

$$u_g + jh_h = u_{ac} e^{j\frac{5}{6}\pi} + u_{bc} e^{j\frac{7}{6}\pi} \quad (10)$$

In addition:

$$\|u_{ac}\| = \|u_{bc}\| \quad (11)$$

Combining equation (10) with (11) yields:

$$u_g = -\frac{\sqrt{3}}{2}(u_{ac} + u_{bc}) \quad (12)$$

$$u_h = \frac{1}{2}(u_{ac} - u_{bc}) \quad (13)$$

According to equations (12) and (13), the sector of the current vector is obtained by determining the sign of $u_{ac}+u_{bc}$ and $u_{ac}-u_{bc}$ without calculating u_g and u_h.

According to Table IV, the total reaction time of the effective basic short vectors (U_0, U_3) in each cycle is:

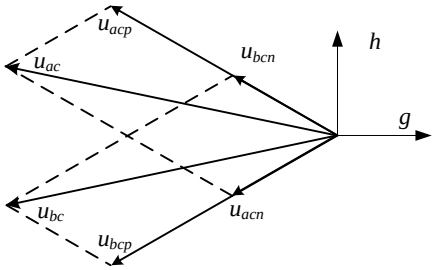

(a) Space vector diagram of line voltage.

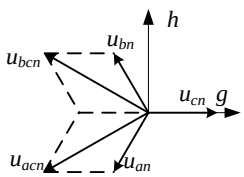

(b) Negative sequence vector.

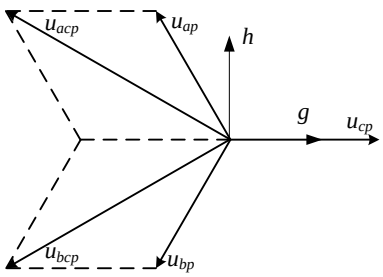

(c) Positive sequence vector.

Fig. 5. Vector diagrams of output voltage.

TABLE IV
JUDGMENT OF SECTOR

Sector	$u_{ac}+u_{bc}$	$u_{ac}-u_{bc}$	U_g	U_h
I	-	+	U_2	U_0
Ⅱ	+	+	U_2	U_3
Ⅲ	+	-	U_1	U_3
Ⅳ	-	-	U_1	U_0

$$t_g = \left|u_{ac}+u_{bc}\right| T_s / 2\sqrt{2}u_{dc} \tag{14}$$

where T_s is the unit time period. The total reaction time of the effective basic long vectors (U_1, U_2) in each cycle is:

$$t_h = \left|u_{ac}-u_{bc}\right| T_s / 2\sqrt{2}u_{dc} \tag{15}$$

When $t_g+t_h>T_s$, $t_g'= t_gT_s/(t_g+t_h)$ and $t_h'= t_hT_s/(t_g+t_h)$ after modification. The action time of the zero vector $t_0=T_s-t_g-t_h$. Since the fundament vectors of the TFSSAPF do not have a zero vector and each of the individual long vectors do not change the equalization voltage of the capacitors, the corresponding long vectors (U_1, U_2) are added up to get the equivalent zero vector. With the zero vector, the study in [18] proposed a five-segment-type SVPWM algorithm. Based on this study, an improved SVPWM modulation algorithm is proposed for the TFSSAPF to reduce the switching frequency.

TABLE V
IMPROVED ALGORITHM OF SVPWM

Sector	$u_{ac}+u_{bc}$	$u_{ac}-u_{bc}$	Action sequence
I	-	+	$U_2\ U_0\ U_1\ U_0\ U_2$
II	+	+	$U_2\ U_3\ U_1\ U_3\ U_2$
III	+	-	$U_1\ U_3\ U_2\ U_3\ U_1$
IV	-	-	$U_1\ U_0\ U_2\ U_0\ U_3$

In addition, according to Fig. 3, only the long vectors do not change the equalization voltage of the capacitors. Therefore, the long vectors are used to get the zero vector. However, the zero vector does not utilize the centralized policy. Therefore, the long vectors are inserted in the middle of the synthesis zero vector. In this method, the phase switching state only changes once per unit time period T_s and there is no interchange between each of the short vectors. Thus, the switching frequency is effectively reduced.

In Table V, the total reaction time of the effective basic long vectors is t_h, the total reaction time of the effective basic short vectors is $(T_s-t_g+t_h)/2$ and the reaction time of the equivalent zero vector is $(T_s-t_g-t_h)/2$. According to Table V and the reaction time of the basic vectors, a timing sequence diagram of the switching signals is shown in Fig. 6.

Fig. 6 shows the timing sequence diagrams of the switching signals from the study in [18] and the proposed method in this paper. In the proposed method, the phase switching state changes only once per unit time period, and the switching state changes when the sector switches between sector II and sector III or between sector IV and sector I. As a result, there are 5 switches in the 4 switching periods of T_s and the switching frequency $f_1=5/(4T_s)$. From the study in [18], the switching state in two sectors changes twice per unit time period. Adding up the changes when the sector switches results in a total of 7 switches in the 4 switching period of T_s and the switching frequency $f_2=7/(4T_s)$. In conclusion, with the equivalent control effect, the switching frequency of the proposed SVPWM method is reduced to 2/7 of the previous method.

IV. DC VOLTAGE CONTROL SCHEME

Since the APF itself is a device which cannot produce (consume) power, the three-phase output current is in equilibrium and the DC-side capacitor voltage does not change when the APF is at the steady state. The problem with the APF DC-side capacitor voltage regulator is equivalent to the problem with the active power balance between the DC-side and the power grid, which has been studied a great deal. The TFSSAPF DC-side voltage stability control method is the same as the three-phase six-switch APF DC-side

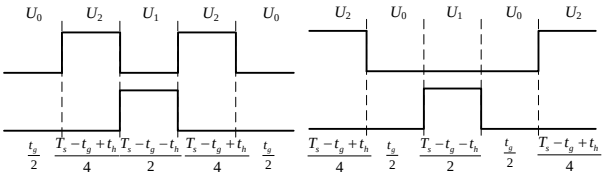

(a) Sector I in the literature [18]. (b) Sector I in this paper.

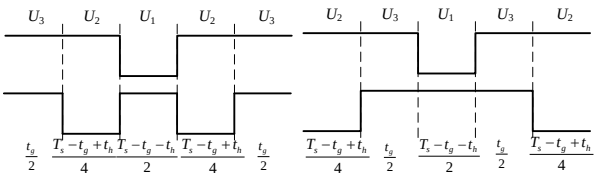

(c) Sector II in the literature [18]. (d) Sector II in this paper.

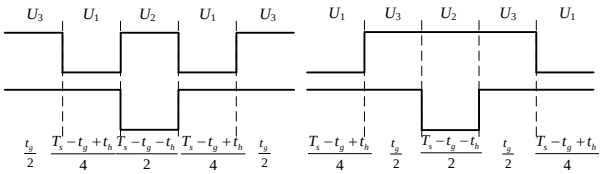

(e) Sector III in the literature [18]. (f) Sector III in this paper.

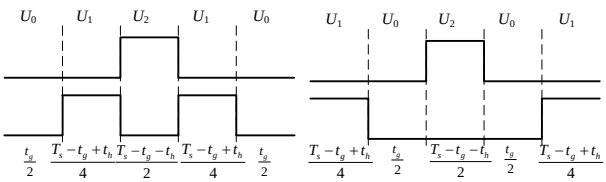

(g) Sector IV in the literature [18]. (h) Sector IV in this paper.

Fig. 6. Timing sequence diagram of the switching signals.

capacitor voltage stability control method, which will not be repeated in this paper.

However, it is worth pointing out that, according to Fig. 4 and Table III, when the reference vector is a quadrilateral inscribed circle composed of basic vectors, the TFSSAPF maximum modulation ratio is $1/2\sqrt{2}$. With the three-phase six-switch APF the maximum modulation ratio is $\sqrt{1/2}$ and the utilization rate of the DC-side voltage is only half that under the normal topology condition. Therefore, in order to achieve the required inverter voltage, the TFSSAPF DC-side voltage should be set to twice the normal value. Taking the increased power loss in the higher DC-side voltage into account, the DC-side voltage general is little less than double.

Since the c-phase bridge is directly connected to the middle of C_1 and C_2, the midpoint voltage is not spontaneously equalized but is affected by the c-phase bridge current. Stabilizing the voltage of the DC-side capacitors is an important issue to guarantee the steady-state compensation accuracy.

According to Fig. 2 and the analysis above, when the power grid contains all three-phase positive sequence components, only the active component in phase c affects the midpoint voltage. Therefore, the active component current

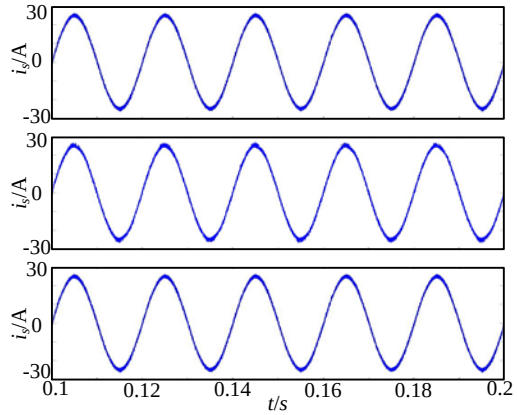

Fig. 7. Grid current after Compensation.

can be controlled in phase c to solve the two capacitors equalization problem. The revised three-phase reference currents are:

$$\begin{cases} i^*_{aref} = i_{aref} \\ i^*_{bref} = i_{bref} \\ i^*_{cref} = i_{cref} + (K_p + K_i \int dt)(u_{c2} - u_{c1}) \end{cases} \tag{16}$$

According to equation (16), when $u_{c2}>u_{c1}$, the active component of i_{cref} increases, which makes u_{c2} decrease. Since $u_{dc}=u_{c1}+u_{c2}$, u_{c1} increases when u_{dc} is stable. Then, $u_{c1}=u_{c2}$ eventually. When $u_{c2}<u_{c1}$, the situation is similar.

V. Simulation and Experimental Results

A. Simulation

To verify the feasibility and correctness of the proposed method in this paper, a TFSSAPF system model based on Matlab/Simulink is established. Assuming that the c-phase circuit is open, the c-phase bridge is directly connected to the middle of the DC side capacitors after fault diagnosis. The simulation parameters are: $C_1=C_2$=6800μF, U_S=220V, U_{dc}=1400V, L_1=1mH, and R_L=23Ω.

Waveforms of the grid current after compensation with the hysteresis control method in the α-β coordinate system proposed in this paper, the SVPWM modulation algorithm proposed in the study in [18], and the improved SVPWM modulation algorithm proposed in this paper are shown in Fig. 7.

According to Fig. 7, both of the methods proposed in this paper can control the TFSSAPF effectively. They both have a good compensation effect and the THD of the grid current after compensation is kept within 5%.

Compared with the study in [18], the improved SVPWM modulation algorithm only changes the sequence of the basic vector output. Thus, one phase switching state changes per unit time period. Fig. 8(a) and Fig. 8(b) show the drive waveforms of the five-segment-type SVPWM modulation

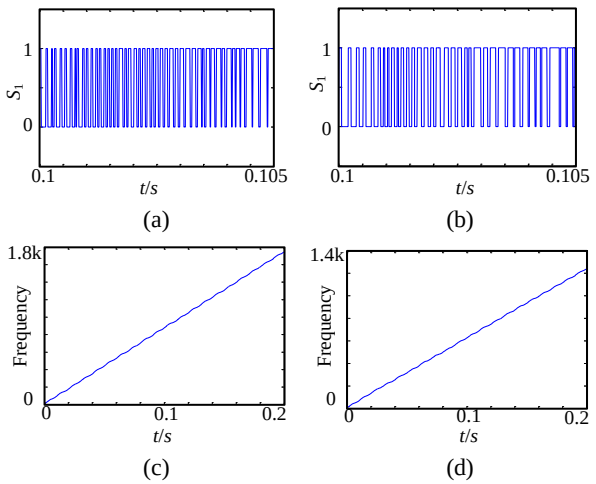

Fig. 8. Waveform of drive signal. (a) Drive signal with the method in the literature [18]. (b) Drive signal with the method in this paper. (c) Switching frequency statistics with the method in the literature [18]. (d) Switching frequency statistics with the method in this paper.

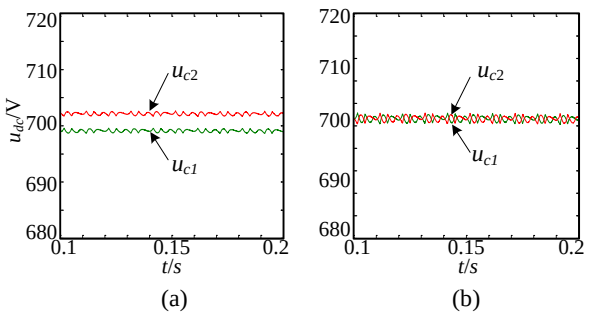

Fig. 9. Waveform of DC voltage. (a) DC-side voltage waveform without equalization scheme. (b) DC-side voltage waveform with equalization scheme.

algorithm proposed in [18] and the improved SVPWM modulation algorithm proposed in this paper, respectively. Fig. 8(c) and Fig. 8(d) shows the switching frequencies of these two methods, respectively.

When T_s=2e-4s, the switching frequency of the traditional five-segment-type SVPWM algorithm in [18] is about 8.75kHz, while the switching frequency of the improved algorithm is about 6.25kHz. This is a reduction of 2/7 as expected. The results without affecting the compensation accuracy are shown in Fig. 7, which also effectively reduces the switching frequency and the switching losses.

In order to verify the DC-side capacitor voltage equalization scheme, through a simulation study, the DC-side capacitor voltage waveform is shown in Fig. 9.

Fig. 9(a) is the waveform without the DC capacitor voltage equalization scheme. The phase c current is not corrected so that u_{c1} and u_{c2} are about 700V. However, this cannot achieve full equalization. Fig. 9(a) is the waveform of that current after revision. The waveforms of u_{c1} and u_{c2} nearly overlap with the setting value of 700V, and the DC-side capacitor voltage gets effectively equalized.

TABLE VI
PARAMETERS OF EXPERIMENT

Parameters	Values
Prototype capacity S/kVA	5
System line voltage U_s/V	380
DC capacitor C/μF	3000
Output filter L/mH	1
Sampling frequency f/kHz	10
DC voltage setting U_{dc}/V	1400

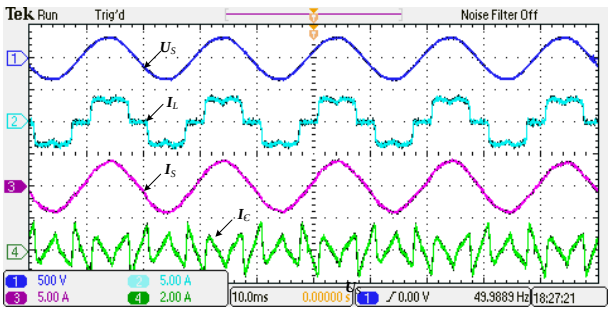

Fig. 10. Current waveform after compensation.

B. Experiment

To further verify the correctness and feasibility of the proposed methods, a 5KW prototype has been implemented in the laboratory. The prototype control unit utilizes a TMS320F28335 DSP chip combined with a FPGA chip EP2C20F256, dual-core for better computing and logic functions. The IGBT modules use Simon Kang SKM400GB176Ds and the IGBT drivers use Simon Kang SKHI23/17(R)s. The prototype experimental parameters are shown in Table VI. The other parameters of the experiment are consistent with the simulation. A TEK oscilloscope DPO2024 and a FLUKE 43B power quality analyzer record the data and waveforms.

Fig. 10 shows the current waveform after a normal three-phase six-switch APF compensation with the hysteresis control method.

According to Fig. 10, the grid current waveform after compensation with the traditional APF topology has no offset, the total harmonic distortion (THD) of the system current drops by 27% to 2.8%, and the low-order harmonics of the non-linear load are effectively eliminated.

When the APF has a phase switch fault, the topology turns to the TFSSAPF. Fig. 11 shows the current waveform after compensation with the hysteresis control method in the α-β coordinate system proposed in this paper.

According to Fig.11, the THD of the system current after compensation is 5.8%. This shows that the TFSSAPF cannot use three independent hysteresis comparators to control the three-phase current. However, the hysteresis current control method can control two-phase stationary coordinates on the α-β axis to achieve complete control of the abc three-phase current. From Fig. 10 and Fig. 11, due to the lack of two

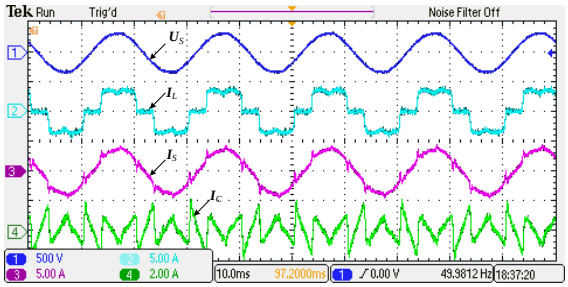

Fig. 11. TFSSAPF waveform after compensation with hysteresis control.

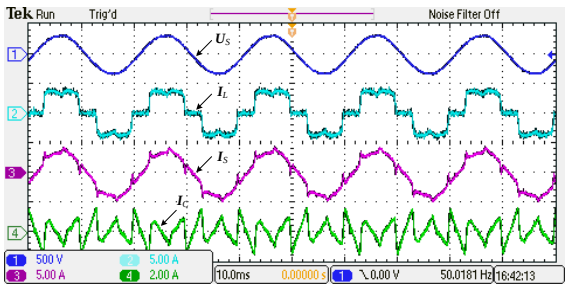

(a) Experimental waveforms in the literature [18].

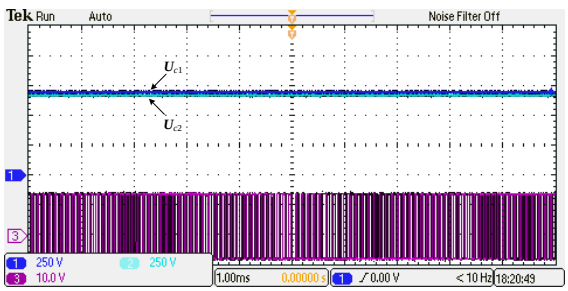

(b) DC voltage and the drive signal in the literature [18].

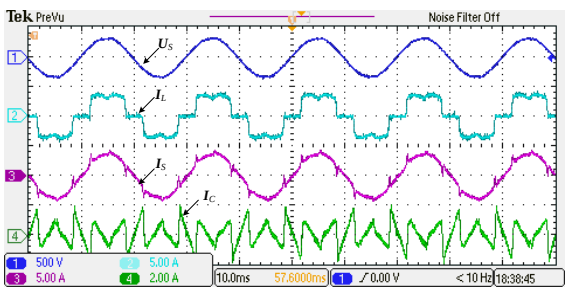

(c) Experimental waveforms in this paper.

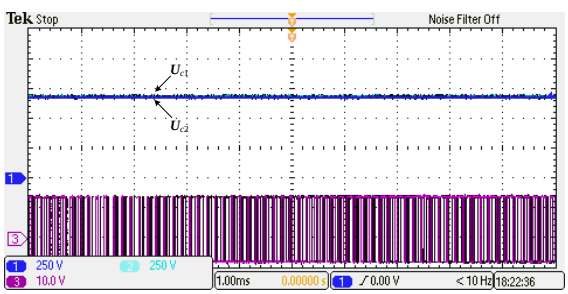

(d) DC voltage and the drive signal in this paper.

Fig. 12. TFSSAPF waveform after compensation with SVPWM control.

switching states, the modulation accuracy of the TFSSAPF is less than the traditional three-phase six-switching APF. However, the results still meet the compensation standards of industrial applications.

Fig. 12 shows the TFSSAPF experimental waveforms after compensation with the SVPWM modulation algorithm. Fig. 12(a) and Fig. 12(b) are the results with the algorithm in [18], and Fig. 12(c) and Fig. 12(d) are results with the improved algorithm and capacitor voltage equalization method in this paper.

From a comparison of Fig. 12(a) and Fig. 12(c), it can be seen that the compensation effects of the two modulation methods are similar, and that the compensated grid current THDs are 6.8% and 6.6%. However, from a comparison of Fig. 12(a) and Fig. 12(c), it can be seen that the improved method effectively reduces the switching frequency to about 5/7 of that in [18]. Fig. 12(b) shows the method without the DC-side capacitor voltage equalization scheme in which there exists a voltage difference between the two capacitors. From Fig. 12(d), it can be seen that the method with the DC-side capacitor voltage equalization scheme makes the DC-side capacitor voltage equalized and stable. The simulation and experimental results are consistent, which further verifies the correctness of the proposed control methods in this paper.

VI. Conclusion

- An APF fault-tolerant topology is adopted and the topology is changed to a TFSSAPF to continue working when there is fault in a single-phase power device.
- A TFSSAPF hysteretic control method in the α-β coordinate system is proposed, which completely controls the three-phase current in the two-phase stationary coordinate system. In addition, the switching state table is given.
- An improved TFSSAPF SVPWM modulation algorithm in *g*-*h* coordinate system is proposed. Only one phase switching state changes within each sector in the improved algorithm, which is simplified and reduces the switching frequency.
- The selection of the TFSSAPF DC-side voltage setting is discussed, and the DC-side capacitor voltage equalization scheme is given.

Acknowledgment

This work was supported by Prospective joint research project of Production, Study and Research, Jiangsu, China (Grant NO: BY2014127-13)

REFERENCES

[1] Z. Shuai, A. Luo, J. Shen, and X. Wang, "Double closed-loop control method for injection-type hybrid active power filter," *IEEE Trans. Power Electron.*, Vol. 26, No. 9, pp. 2393-2403, Sep. 2011.

[2] J. He, Y. Li, F. Blaabjerg, and X. Wang, "Active harmonic filtering using current-controlled, grid-connected DG units with closed-loop power control," *IEEE Trans. Power Electron.*, Vol. 29, No. 2, pp. 642-653, Feb. 2014.

[3] Z. F. Zobaa, "Optimal multiobjective design of hybrid active power filters considering a distorted environment," *IEEE Trans. Ind. Electron.*, Vol. 61, No. 1, pp. 107-114, Jan. 2014.

[4] P. Acuna, L. Moran, M. Rivera, and J. Dixon, "Improved active power filter performance for renewable power generation systems," *IEEE Trans. Power Electron.*, Vol. 29, No. 2, pp. 687-694, Feb. 2014.

[5] W. Dong, X. Bai, N. Zhu, Z. Zhou, H. Li, and W. Li, "Research on fault diagnosis and fault tolerant control of active power filters," *Proceedings of the CSEE*, Vol. 33, No. 18, pp. 65-72, 2013.

[6] T. Ghennam, E. M. Berkouk, and B. Francois, "A novel space-vector current control base on circular hysteresis areas of a three-phase neutral-point-clamped inverter," *IEEE Trans. Ind. Electron.*, Vol. 57, No. 8, pp. 2669-2678, Aug. 2010.

[7] A. Garcia-Cerrada, O. Pinzon-Ardila, V. Feliu-Batlle, P. Roncero-Sanchez, and P. Garcia-Gonzalez, "Application of a repetitive controller for a three-phase active power filter," *IEEE Trans. Power Electron.*, Vol. 22, No. 1, pp. 237-245, Jan. 2007.

[8] C. Ramon, R. Grino, and E. Fossas, "Odd-harmonic digital repetitive control of a single-phase current active filter," *IEEE Trans. Power Electron.*, Vol. 19, No. 4, pp. 1060-1068, Jul. 2004.

[9] K. Zhou and D. Wang, "Unified robust zero-error tracking control of CVCF PWM converters," *IEEE Trans. Circuits Syst. I, Fundam. Theory Appl.*, Vol. 49, No. 4, pp. 492-501, Apr. 2002.

[10] M. N. Uddin, T. S. Radwan, and M. A. Rahman, "Fuzzy-logic-controller-based cost-effective four-switch three-phase inverter-fed IPM synchronous motor drive system," *IEEE Trans. Ind. Appl.*, Vol. 42, No. 1, pp. 21-30, Jan. 2006.

[11] C. Xia, Z. Li, and T. Shi, "A control strategy for four-switch three-phase brushless DC motor using single current sensor," *IEEE Trans. Ind. Electron.*, Vol. 56, No. 6, pp. 2058-2066, Jun. 2009.

[12] T. Lee and J. Liu, "Modeling and control of a three-phase four-switch PWM voltage-source rectifier in *d-q* synchronous frame," *IEEE Trans. Power Electron.*, Vol. 26, No. 9, pp. 2476-2489, Sep. 2011.

[13] Q. Trinh and H. Lee, "An advanced current control strategy for three-phase shunt active power filters," *IEEE Trans. Ind. Electron.*, Vol. 60, No. 12, pp. 5400-5410, Dec. 2013.

[14] X. Tan, Q. Li, H. Wang, L. Cao, and S. Han, "Variable parameter pulse width modulation-based current tracking technology applied to four-switch three-phase shunt active power filter," *IET Power Electron.*, Vol. 6, No. 3, pp. 543-553, Mar. 2013.

[15] H. Liu, S. Lu, and C. Zhang, "Space vector pulse width modulation of three-phase four-switch shunt active power filter," *Trans. China Electrotechnical Society*, Vol. 26, No. 4, pp. 128-134, 2011.

[16] H. Liu and J. Peng, "Study on current command signal of three-phase four-switch shunt active power filter," *Trans. China Electrotechnical Society*, Vol. 29, No. 26, pp. 108-113, 2009.

[17] W. Wang, A. Luo, Y. Li, X. Xu, L. Fang, J. Wu, and F. Fan, "A novel algorithm of SVPWM applied to active power filters," *Proc. the CSEE*, Vol. 32, No. 18, pp. 52-58, 2012.

[18] W. Wang, A. Luo, X. Xu, and L. Fang, "Space vector pulse-width modulation algorithm and DC-side voltage control strategy of three-phase four-switch active power filters," *IET Power Electron.*, Vol. 6, No. 1, pp. 125-135, Jan. 2013.

[19] K. Nishida, M. Rukonuzzman, and M. Nakaoka, "Advanced current control implementation with robust deadbeat algorithm for shunt single-phase voltage-source type active power filter," *IEE Proc.-Electr. Power Appl.*, Vol. 151, No. 3, pp. 283-288, 2004

Chenyu Zhang was born in Jiangsu, China. He received his B.S. degree in Electrical Engineering from Hunan University (HNU), Changsha, China, in 2011. He is now pursuing his Ph.D. degree in Electrical Engineering at Southeast University (SEU), Nanjing, China. His current research interests include micro-grid power quality, harmonic suppression and the digital control of power converters.

Jianyong Zheng was born in China, in 1966. He received his B.S., M.S., and Ph.D. degrees from the School of Electrical Engineering, Southeast University, Nanjing, China, in 1988, 1991, and 1999, respectively. He is now a Full Professor in the School of Electrical Engineering, Southeast University. His current research interests include the application of power electronics in power systems and renewable energy technology.

Jun Mei received his B.S. degree in Radio Engineering from Chongqing University, Chongqing, China, in 1994, and his M.S. and Ph.D. degrees in Electrical Engineering from Southeast University, Nanjing, China, in 2001 and 2006, respectively. He is now an Associate Professor in the School of Electrical Engineering, Southeast University. From 2011 to 2012, he was a Visiting Scholar at the University of Tennessee, Knoxville, TN, USA. His current research interests include electric power converters for distributed energy sources, FACTS and power quality control.

Kai Deng was born in Jiangsu, China. He received his B.S. degree from the Nanjing Agricultural University (NAU), Nanjing, China, in 2009, and his M.S. degree from the Beijing Institute of Technology (BIT), Beijing, China, in 2012, both in Electrical Engineering. He is now pursuing his Ph.D. degree in Electrical Engineering at

Southeast University (SEU), Nanjing, China. His current research interests include Z-source inverters, the digital control of power converters and the system integration of modular power converters.

Fuju Zhou was born in Jiangsu, China, in 1990. He received his B.S. degree in Electrical Engineering from the Nanjing University of Science and Technology (NJUST), Nanjing, China. He is now pursuing his M.S. degree in Electrical Engineering at Southeast University (SEU), Nanjing, China. His current research interests include power system harmonic suppression and reactive power compensation.